Design and analysis of electrically calibrated tympanic thermometers

Mang Ou-Yang, Jin-Shown Shie, and Chyi Tsao

A new tympanic thermometer is analyzed and tested experimentally. An electrically calibrated pyroelectric detector of special configuration is employed to determine a person's body temperature. An energy-storage, power-supply-isolated capacitor is used as the electrical heating reference. The new thermometer design has an accuracy within ±0.1 °C with a 90% confidence and is immune to ambient temperature, detector aging, and parameter variations. An equivalent-circuit model is established in the analysis to account for the heat exchanges among the tympanum, the surroundings, and the detector as well as for the electrothermal behavior of the detector. The model provides effective simulation of the thermometer with PSPICE. Critical parameters governing the accuracy and the limitation of the tympanic thermometer are also pointed out by the simulation. © 1998 Optical Society of America

OCIS codes: 040.3060, 120.6780, 120.5630, 170.3890.

1. Introduction

The temperature, the heart rate, the blood pressure, and the respiratory rate of human beings are the four traditional cardinal vital signs from a medical point of view. Physiologically, one's temperature represents the mixed body heat generated in one's metabolically active organs and subcutaneous tissues. Medically, the internal human-body temperature is called the core temperature, which is normally maintained within 37 ± 0.75 °C (Ref. 1) by blood, the heat transport medium. Clinically, medical professionals have long been interested in accurately monitoring the core temperature of patients, primarily because temperature measurement is the first step in understanding the patient's condition, and the diagnosis or the treatment of many diseases depends on the accuracy of the core-temperature reading. So far, various ways of measuring core temperature have been developed, including mercury and electronic thermometers, a probe with an esophagal stethoscope, bladder, and pulmonary artery probes.[1] However, there are drawbacks to using these techniques practically. Invasive insertion, long measurement time, accuracy, and selection of the correct probe site are the main concerns. A quick and precise method for measuring the core temperature at a noninvasive site is required in modern clinical applications.

Benzinger in 1959[2] first proposed the human tympanic membrane as the ideal site for core-temperature measurement, and many reports have confirmed this.[3–8] This membrane is ideal because it is located near the carotid artery and shares the same blood supply as the hypothalamus, which controls body temperature. The temperature of the tympanum has been proved to be highly correlated with that of the esophagus and the pulmonary artery and is a golden standard for core-temperature measurements.[3]

Noncontact tympanic thermometers capable of measuring IR radiation from the eardrum through the ear canal are noninvasive. Of growing importance for both clinical and homecare use is that most of these thermometers use thermal detectors, such as pyroelectric detectors or thermopiles, because of their wide-band absorption and low cost.[4,5] However, owing to the intrinsic characteristics associated with these thermal detectors, in many clinical articles problems have been reported with these systems.[6–8] For example, Jakobsson *et al.*[6] compared the clinical measurements from the thermometers of four different brands and found that they differ by as much as 1 °C. In addition, in other articles the results reported depend on the ambient temperature during a

M. Ou-Yang and J.-S. Shie are with the Institute of Electro-Optical Engineering, National Chiao Tung University, Hsinchu, Taiwan. C. Tsao is with Oriental System Technology Inc. and Hsinchu Science-Based Industrial Park, Hsinchu, Taiwan.

Received 10 October 1997; revised manuscript received 1 December 1997.

0003-6935/98/132708-08$15.00/0

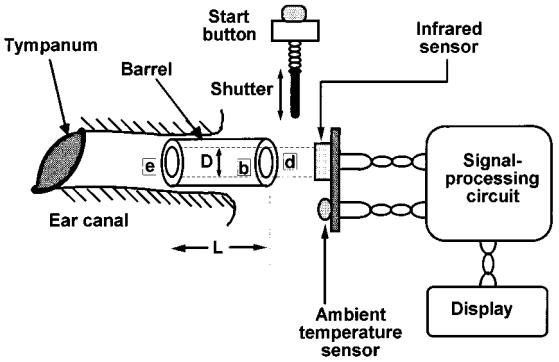

Fig. 1. Schematic diagram of the tympanic thermometry.

measurement. Therefore, to avoid the influence of environmental changes or detector aging, various calibration methods are required before each use of these thermometers.

In this paper, a new pyroelectric-type tympanic thermometer is described. Basically, the device employs the principle of the electrically calibrated pyroelectric radiometer (ECPR) developed at NIST.[9,10] A pyroelectric detector with a coated surface heater is heated electrically until its response signal equals that of an unknown radiation previously incident upon the detector. The amount of electrical power is measured and used to represent the unknown radiant power. Since electrical power can be measured much more accurately than any optical quantity, the ECPR has been classified as a detector-based absolute standard for radiometry.[11] However, in the NIST method, continuous and long-time chopping is necessary to adjust the electrical heating power at an autonulled state. This process is not suitable for tympanic thermometry, which usually requires quick measurements for clinical convenience. In the modified method presented here, new circuits and algorithms are designed to provide a single heating pulse for each measurement. An electrically calibrated pyroelectric (ECP) detector of special configuration is made for the new tympanic thermometer. In addition, an opto-electro-thermal PSPICE model that includes the radiation network, the sensor, and the electrical circuit is developed for an integrated simulation of tympanic thermometry.

2. Tympanic Thermometry

A. Description

The internal structure of a human ear and a tympanic thermometer are represented schematically in Fig. 1. The thermometer consists mainly of five parts, an IR sensor, a barrel, a shutter, an ambient-temperature sensor, and the associated circuit. The ear canal guides sound to the eardrum, which is thin and flooded with blood at the core temperature. The barrel, usually a cylindrical pipe with a highly reflective inner surface for confining the radiation, is adaptive to the outer canal without contacting the eardrum. The shutter controls whether the flux is transferred to the IR sensor. When the shutter is open, radiative fluxes transfer among the tympanum, the IR sensor, and the inner surface of the barrel. The ambient sensor is mounted near the IR sensor to monitor the ambient temperature.

To measure core temperature, a tympanic thermometer is inserted into a patient's outer ear canal. A start button is pressed to open the shutter momentarily and to start the measurement through the radiation exchanges. The electrical signal read out from the detector is fed to the circuit for amplification and calculation. The measured temperature then appears on a display. The total operation takes a few seconds.

The tympanic temperature can be determined by the net radiative flux falling on the IR sensor $\mathbf{Q}_d$, and the ambient or detector temperature $\mathbf{T}_d$. In steady state, the tympanic temperature $\mathbf{T}_e$ can be calculated according to the blackbody radiation law and conservation of energy and reads[12]

$$\mathbf{T}_e = \left(\frac{c\mathbf{Q}_d}{\varepsilon_d\varepsilon_e} + \mathbf{T}_d{}^4\right)^{1/4} = \left(\frac{c\mathbf{V}_s}{\varepsilon_d\varepsilon_e\Re_v} + \mathbf{T}_d{}^4\right)^{1/4}, \qquad (1)$$

with $\mathbf{Q}_d = \mathbf{V}_s/\Re_v$. Here $\Re_v$ is the detector voltage responsivity, $\mathbf{V}_s$ is the detector output voltage, ε is the emissivity, and $\mathbf{T}$ is the absolute temperature. Subscripts e and d denote the eardrum and the detector, respectively, and c is a constant related to device geometry and parameters. Hence, to measure the eardrum temperature $\mathbf{T}_e$, one must know the instantaneous detector temperature $\mathbf{T}_d$ and calibrate the product of constants $c/(\varepsilon_e\varepsilon_d\Re_v)$.

The product of constants can vary with time and measurement conditions. Chronic variation of the detector responsivity $\Re_v$ is the most troublesome. $\Re_v$ is generally influenced by ambient temperature and detector aging. Therefore the device requires constant calibration during use. Also, to avoid measurement errors resulting from the effects of the temperature drift of the barrel and the sensor substrate (the ambient-temperature effect), the outer part of the barrel is surrounded with plastic material serving as the thermal blanket and the inner surface is optically polished to reduce its emissivity. However, since the ambient-temperature effect is still large compared with the weak radiation signal on the detector, its influence demands more careful analytical study.

B. Radiant Heat Exchanges

When one is designing a noncontact tympanic thermometer, it is most important to estimate the content of the net radiant flux on the IR sensor, $\mathbf{Q}_d$. The detector receiving flux both from the tympanum and from the inner surface of the barrel complicates this estimate. This surface not only emits radiation by itself but also reflects that from the outside. A model that describes the radiant exchanges among all surfaces has been developed to clarify the role of the barrel on tympanic temperature measurements.

To begin, for the simple case of radiant exchange

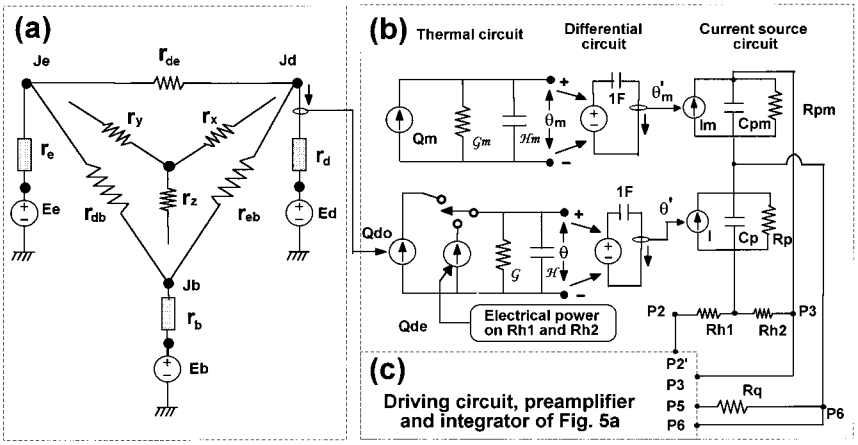

Fig. 2. Opto-electro-thermal PSPICE model of the present tympanic thermometer: (a) radiant network model, (b) electrothermal model of the pyroelectric sensor model, and (c) associated circuit.

from an opaque diffusive surface i of area A_i and emissivity ε_i, the net increased flux on the surface $\mathbf{Q}_i$ can be expressed as

$$\mathbf{Q}_i = \frac{\varepsilon_i}{1-\varepsilon_i}\mathbf{A}_i(\mathbf{J}_i - \mathbf{E}_i) = \frac{1}{\mathbf{r}_i}(\mathbf{J}_i - \mathbf{E}_i), \tag{2}$$

where $\mathbf{r}_i^{-1} = \mathbf{A}_i\varepsilon_i/(1-\varepsilon_i)$ is defined as the surface resistance.[13] Here $\mathbf{J}_i$ is the total exitance; $\mathbf{E}_i$ is the blackbody emittance, which is $\sigma\mathbf{T}_i^4$; and σ is the Stefan–Boltzmann constant. For the case of radiation exchange between two separate surfaces, $\mathbf{A}_i$ and $\mathbf{A}_j$, the flux quantity transferred from **i** to **j**, $\mathbf{Q}_{ij}$ can be written as[14]

$$\mathbf{Q}_{ij} = \mathbf{J}_i\mathbf{A}_i\mathbf{F}_{ij}, \tag{3}$$

with

$$\mathbf{F}_{ij} = \frac{1}{\mathbf{A}_i}\int_{\mathbf{A}_i}\int_{\mathbf{A}_j}\frac{\cos\theta_i\cos\theta_j}{\pi\mathbf{R}_{ij}^2}\,d\mathbf{A}_i d\mathbf{A}_j. \tag{4}$$

Here $\mathbf{R}_{ij}$ is the distance between the two surfaces, θ_i and θ_j are the projected angles between $\mathbf{R}_{ij}$ and the two surface normals, and $\mathbf{F}_{ij}$ is called the view factor that obeys the reciprocity,

$$\mathbf{A}_i\mathbf{F}_{ij} = \mathbf{A}_j\mathbf{F}_{ji}. \tag{5}$$

Extending the exchange theory to an enclosure comprising $N+1$ surfaces, **i** and **j** ranging from 1 to N, the net increased flux on the surface **i** can be derived, with the aid of the identity

$$\sum_{j=1}^{N}\mathbf{F}_{ij} \equiv 1 \tag{6}$$

as

$$\begin{aligned}\mathbf{Q}_i &= \sum_{j=1}^{N}\mathbf{A}_j\mathbf{F}_{ji}\mathbf{J}_j - \mathbf{A}_i\mathbf{J}_i \\ &= \sum_{j=1}^{N}\mathbf{A}_i\mathbf{F}_{ij}(\mathbf{J}_j - \mathbf{J}_i) \\ &= \sum_{j=1}^{N}\frac{1}{\mathbf{r}_{ij}}(\mathbf{J}_j - \mathbf{J}_i),\end{aligned} \tag{7}$$

where $\mathbf{r}_{ij}^{-1} = \mathbf{A}_i\mathbf{F}_{ij}$ is the space resistance.[13]

C. Radiation-Network Modeling

A radiation network can be set up to represent Eqs. (2) and (7). $\mathbf{E}_i$ and $\mathbf{J}_i$ are equivalent to an independent voltage source and a node potential, respectively; $\mathbf{Q}_i$ is equivalent to a branch current from $\mathbf{J}_i$ to $\mathbf{E}_i$; and the surface and space resistances, $\mathbf{r}_i$ and $\mathbf{r}_{ij}$, are analogs of the electrical resistances. This analogy allows direct application of the popular PSPICE circuit simulation tool to simulate radiation-transfer problems.

As shown in Fig. 1, when the shutter is open the front and backsides and the inner surface of the cylindrical barrel form an enclosure. The front surface, **e**, is considered to be an effective surface standing for the tympanum with assumed unit emissivity. This assumption is justified by the fact that human tissue has a high emissivity of ~0.99 (Ref. 15) and that the inner tympanic cavity forms a blackbody[12] that prevents reflection of radiation emitted from the front barrel. The backside surface, **d**, where the IR sensor is installed is assumed to be the absorption layer of the IR sensor. Therefore the three surfaces, **e**, **d**, and **b**, constitute a closed radiant network that can be treated with Eqs. (2) and (7). The correspondent equivalent-circuit model is shown in Fig. 2(a).

Suppose the cylindrical barrel has a length **L** and a diameter **D**. Then the view factor between the detector and the eardrum, $\mathbf{F}_{de}$, can be written as[14]

$$\mathbf{F}_{de} = 1 + \frac{2\mathbf{L}^2}{\mathbf{D}^2} - \frac{2}{\mathbf{D}}[\mathbf{L}(\mathbf{D}+\mathbf{L})]^{1/2}. \tag{8}$$

The other two view factors, $\mathbf{F}_{db}$ and $\mathbf{F}_{eb}$, equal each other because of the symmetric geometry, and by Eq. (6),

$$\mathbf{F}_{db} = \mathbf{F}_{eb} = 1 - \mathbf{F}_{de}. \tag{9}$$

Substituting Eqs. (8) and (9) into Eq. (7), we can write the space resistances $\mathbf{r}_{de}$, $\mathbf{r}_{db}$, and $\mathbf{r}_{eb}$ of the tympanic enclosure in more detail.

We can solve the net flux absorbed by the IR sensor,

$\mathbf{Q}_d$, by using $\Delta - Y$ transformations. The results give the three branches of a Y network:

$$\mathbf{r}_x = \frac{\mathbf{r}_{de}\mathbf{r}_{eb}}{\mathbf{r}_{de} + \mathbf{r}_{eb} + \mathbf{r}_{db}}, \tag{10a}$$

$$\mathbf{r}_y = \frac{\mathbf{r}_{de}\mathbf{r}_{db}}{\mathbf{r}_{de} + \mathbf{r}_{eb} + \mathbf{r}_{db}}, \tag{10b}$$

$$\mathbf{r}_z = \frac{\mathbf{r}_{db}\mathbf{r}_{eb}}{\mathbf{r}_{de} + \mathbf{r}_{eb} + \mathbf{r}_{db}}, \tag{10c}$$

as shown in Fig. 2(a). Hence

$$\begin{aligned}\mathbf{Q}_d &= \mathbf{G}_e\mathbf{E}_e + \mathbf{G}_b\mathbf{E}_b + \mathbf{G}_d\mathbf{E}_d \\ &= \mathbf{G}_e\sigma\mathbf{T}_e^{\,4} + \mathbf{G}_b\sigma\mathbf{T}_b^{\,4} + \mathbf{G}_d\sigma\mathbf{T}_d^{\,4}\end{aligned} \tag{11}$$

with

$$\mathbf{G}_e = \frac{\mathbf{r}_z + \mathbf{r}_b}{(\mathbf{r}_d + \mathbf{r}_x)(\mathbf{r}_z + \mathbf{r}_b) + (\mathbf{r}_y + \mathbf{r}_e)(\mathbf{r}_z + \mathbf{r}_b + \mathbf{r}_d + \mathbf{r}_x)}, \tag{12a}$$

$$\mathbf{G}_b = \frac{\mathbf{r}_y + \mathbf{r}_e}{(\mathbf{r}_d + \mathbf{r}_x)(\mathbf{r}_y + \mathbf{r}_e) + (\mathbf{r}_z + \mathbf{r}_b)(\mathbf{r}_y + \mathbf{r}_e + \mathbf{r}_d + \mathbf{r}_x)}, \tag{12b}$$

$$\mathbf{G}_e = -\frac{\mathbf{r}_z + \mathbf{r}_b + \mathbf{r}_y + \mathbf{r}_e}{(\mathbf{r}_z + \mathbf{r}_b)(\mathbf{r}_y + \mathbf{r}_e) + (\mathbf{r}_d + \mathbf{r}_x)(\mathbf{r}_z + \mathbf{r}_b + \mathbf{r}_y + \mathbf{r}_e)}. \tag{12c}$$

Note that $\mathbf{G}_e + \mathbf{G}_b + \mathbf{G}_d = 0$, which is a natural result of the conservation of energy, and can be proved simply by setting all the surfaces to be isothermal.

The core temperature $\mathbf{T}_e$ therefore can be determined from Eq. (11) as

$$\mathbf{T}_e = \left(\frac{\mathbf{Q}_d}{\sigma\mathbf{G}_e} - \frac{\mathbf{G}_d}{\mathbf{G}_e}\mathbf{T}_d^{\,4} - \frac{\mathbf{G}_b}{\mathbf{G}_e}\mathbf{T}_b^{\,4}\right)^{1/4}. \tag{13}$$

This equation is more complete than the simple theory of Eq. (1), because the barrel temperature has been included. The relative roles of $\mathbf{T}_d$ and $\mathbf{T}_b$ in determining the net radiation $\mathbf{Q}_d$ therefore are more accurately expressed.

D. Temperature Effect of the Barrel

If we assume that $\mathbf{T}_b = \mathbf{T}_d = \mathbf{T}_a$, owing to the closeness of the barrel and the sensor, $\mathbf{T}_e$ can be simplified to

$$\mathbf{T}_e = \left(\frac{\mathbf{Q}_d}{\sigma\mathbf{G}_e} + \mathbf{T}_a^{\,4}\right)^{1/4} = \left(\frac{1}{\sigma\mathbf{G}_e}\frac{\mathbf{V}_s}{\Re_v} + \mathbf{T}_a^{\,4}\right)^{1/4}. \tag{14}$$

Equation (14) expresses explicitly the calibration factor c in Eq. (1). In reality, this assumption is seldom correct unless the temperatures of the barrel and the ear canal are identical. Contact between the two solids causes heat transfer across the barrel due to their temperature difference. The average temperature of the barrel thus is time-varying during measurements, and Eq. (14), which is based on the assumption of identical temperatures, may not be accurate enough. Unfortunately, the temperature drift of the barrel during the measurement is difficult to predict; hence it is important to design a barrel that can make the drift effect small enough to be acceptable or even ignored.

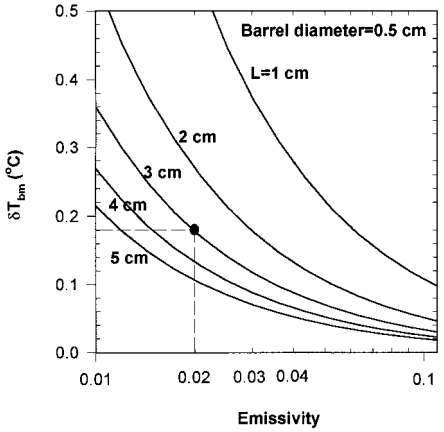

Fig. 3. Plot of the maximal allowable temperature drift δT_{bm} of the barrel with different inner surface emissivities and lengths. When these are 0.02 and 3 cm, respectively, δT_{bm} is 0.18 °C as indicated by the dot point.

Suppose that initially $\mathbf{T}_b = \mathbf{T}_d = \mathbf{T}_a$ and the temperature of the barrel changes a small amount, $\delta\mathbf{T}_b$, after ear contact; then by differentiation of Eq. (13),

$$\delta\mathbf{T}_e = -\frac{\mathbf{G}_b}{\mathbf{G}_e}\cdot\mathbf{T}_b^{\,3}\cdot\left(\frac{\mathbf{Q}_d}{\sigma\mathbf{G}_e} - \frac{\mathbf{G}_d}{\mathbf{G}_e}\mathbf{T}_d^{\,4} - \frac{\mathbf{G}_b}{\mathbf{G}_e}\mathbf{T}_b^{\,4}\right)^{-3/4}\Bigg|_{\mathbf{T}_a}\cdot(\delta\mathbf{T}_b) \tag{15}$$

In medical thermometry, $\delta\mathbf{T}_e$ is generally expected to be within 0.1 °C. In addition, human temperature is normally meaningful between 30 and 43 °C.[1] Temperatures outside this range are vitally dangerous. Furthermore the working ambient-temperature range of a commercial tympanic thermometer is generally defined from 24 to 45 °C. The worst case of Eq. (15) is that $\mathbf{T}_e$ = 30 °C (303 K) and $\mathbf{T}_a$ = 45 °C (318 K). Accordingly, the drift of the barrel is limited to a maximal value,

$$|\delta\mathbf{T}_{bm}| = |\delta\mathbf{T}_e|\cdot\left(\frac{\mathbf{T}_e}{\mathbf{T}_a}\right)^3\cdot\left|\frac{\mathbf{G}_e}{\mathbf{G}_b}\right| = 0.095\times\left|\frac{\mathbf{G}_e}{\mathbf{G}_b}\right|. \tag{16}$$

The maximal allowable drift of the barrel temperature is ~10% of the ratio of $\mathbf{G}_e$ to $\mathbf{G}_b$. These two quantities, which appeared in Eqs. (12a) and (12b), are a complicated function of the various parameters of a tympanic network. Therefore it is more convenient to apply the PSPICE simulation tools directly to the model shown in Fig. 2. The results of the simulation in various conditions are shown in Fig. 3. On the one hand, when the barrel length is fixed, the maximal allowable drift decreases rapidly with increasing emissivity of the inner surface of the barrel. This is obvious since the radiance from the barrel will increase. On the other hand, the allowable drift in-

creases with a shorter barrel, because the IR sensor perceives a larger field of view. Thus one can conclude that a shorter barrel length and a higher reflectance on the inner surface of the barrel are desirable. However, the length is limited by the canal geometry, whereas the reflectance depends on coating quality. For a reasonable length of 3 cm and a reflectance of 0.98 by the gold coating,[15] $\delta\mathbf{T}_b$ is tolerable to as high as 0.18 °C, as indicated in Fig. 3. According to our theoretical prediction, a plastic case surrounding the barrel can successfully restrict the average temperature variation of the barrel below 0.05 °C for a 10-s measurement period.

3. Electrically Calibrated Design

To analyze the detecting mechanics of the pyroelectric sensor, we require a heat-flow and a charge-flow equation[16,17]:

$$\mathcal{H}\frac{\mathrm{d}\theta(t)}{\mathrm{d}t} + \mathcal{G}\theta(t) = \mathbf{Q}_d(t), \tag{17}$$

$$\mathbf{C}_L\frac{\mathrm{d}V(t)}{\mathrm{d}t} + \frac{1}{\mathbf{R}_L}\mathbf{V}(t) = p\mathbf{A}_d\frac{\mathrm{d}\theta(t)}{\mathrm{d}t}. \tag{18}$$

Here $\mathcal{H}$ and $\mathcal{G}$ denote the thermal capacitance and the conductance of the sensor, $\mathbf{C}_L$ and $\mathbf{R}_L$ are the output capacitance and the resistance, p is the pyroelectric coefficient, $\mathbf{A}_d$ is the detector area, and $\mathbf{V}(t)$ is the output voltage. The detector receiving power $\mathbf{Q}_d$ defined in Eq. (11) generates the excess temperature $\theta(t)$. The net irradiance on the detector is expressed by

$$\mathbf{Q}_d(t) = \mathbf{Q}_{do}[u(t) - u(t - t_o)], \tag{19}$$

where $u(t)$ is the unit step function, $\mathbf{Q}_{do}$, is the amplitude, and t_o is the one-shot period. Substituting Eqs. (17) and (19) into Eq. (18), we read the final signal for integration-mode operation as

$$\begin{aligned} S_o &= \int_0^{t_o} V(t)\mathrm{d}t \\ &= \left\{\frac{p\mathbf{A}_d}{\mathbf{C}_L\mathcal{H}}\left(\frac{\tau_e\tau_t}{\tau_e - \tau_t}\right)\left[-\tau_e\exp\left(-\frac{t_o}{\tau_e}\right) + \tau_t\exp\left(-\frac{t_o}{\tau_t}\right) + \tau_e - \tau_t\right]\right\}\cdot\mathbf{Q}_{do} \\ &= \Re_v\cdot\mathbf{Q}_{do}, \end{aligned} \tag{20}$$

where

$$\tau_e = \mathbf{R}_L\mathbf{C}_L, \qquad \tau_t = \mathcal{H}/\mathcal{G}, \tag{21}$$

are the detector electrical and thermal time constants, respectively. The voltage responsivity $\Re_v$ is defined in the parentheses of Eq. (20).

By substituting Eq. (20) into Eq. (14), we can obtain the core temperature explicitly. The measured value therefore depends on the detector responsivity, which is influenced by the electrical and the thermal parameters contained in Eq. (20). However, these parameters vary with manufacturing processes; hence $\Re_v$ varies from detector to detector. Furthermore material aging also produces long-term changes in each detector, especially aging of the pyroelectric coefficient. Therefore initial factory calibration will not suffice for long-term use. As proposed in many articles,[4,5,12] it becomes necessary to calibrate the instrument before every measurement. This often leads to complex circuitry in practical situations.

To solve this problem, we propose an electrically calibrated method that is both accurate and simple in circuit design. With the present method, an artificial electric pulse is applied to a thin-film heater coated on the sensor surface following exposure to the eardrum radiation. The response of the electric pulse is integrated for a duration identical to the optical exposure t_o in Eq. (19). This gives an electrical signal of $\mathbf{S}_e$ similar to Eq. (20), and the radiation energy can be calibrated proportionally. Equation (14) then can be expressed by

$$\mathbf{T}_e = \left(\frac{\mathbf{Q}_{de}}{\sigma\mathbf{G}_e}\frac{\mathbf{S}_o}{\mathbf{S}_e} + \mathbf{T}_a{}^4\right)^{1/4}. \tag{22}$$

Note that this $\mathbf{Q}_{de}$ is the electrical power applied on the heater for a calibration reference and can be measured precisely. The measured core temperature $\mathbf{T}_e$ thus is independent of the responsivity variations discussed previously.

One could also use Eqs. (17) and (18) to establish a PSPICE equivalent circuit to represent the electrothermal behavior of the pyroelectric sensors.[18,19] This is shown in Fig. 2(b), where lump representations are used for both the thermal parameters, $\mathcal{H}$ and $\mathcal{G}$, and the electrical parameters, $\mathbf{C}_p$ and $\mathbf{R}_p$. The subscript m represents the dummy parts as shown in Fig. 2(b). The induced pyroelectric current is represented by a current source $\mathbf{I}$ controlled by the temperature difference θ' from the output of the thermal circuit through a differentiator. Two current-controlled current sources represent the heat power from radiation ($\mathbf{Q}_{do}$) and the electrical heating power ($\mathbf{Q}_{de}$).

With such representations, both the radiation exchange and the thermal properties of the sensor can be incorporated with regular electrical circuits into an integrated circuit model as shown completely in Fig. 2. This allows tools such as PSPICE to be used directly for system simulation. The opto-electrothermal PSPICE model is invaluable to a system engineer in obtaining optimal design for a tympanic thermometer.

4. Experiments and Results

A. Electrically Calibrated Pyroelectric Detector

The electrically calibrated pyroelectric detector for the experiment is shown in Fig. 4. The sensor contains two pyroelectric elements made of $LiTaO_3$, an active one and a dummy, with both floating. A high impedance resistance is used as the output load. All these are mounted on a printed circuit board (PCB) and packed into a TO-metal can structure. This de-

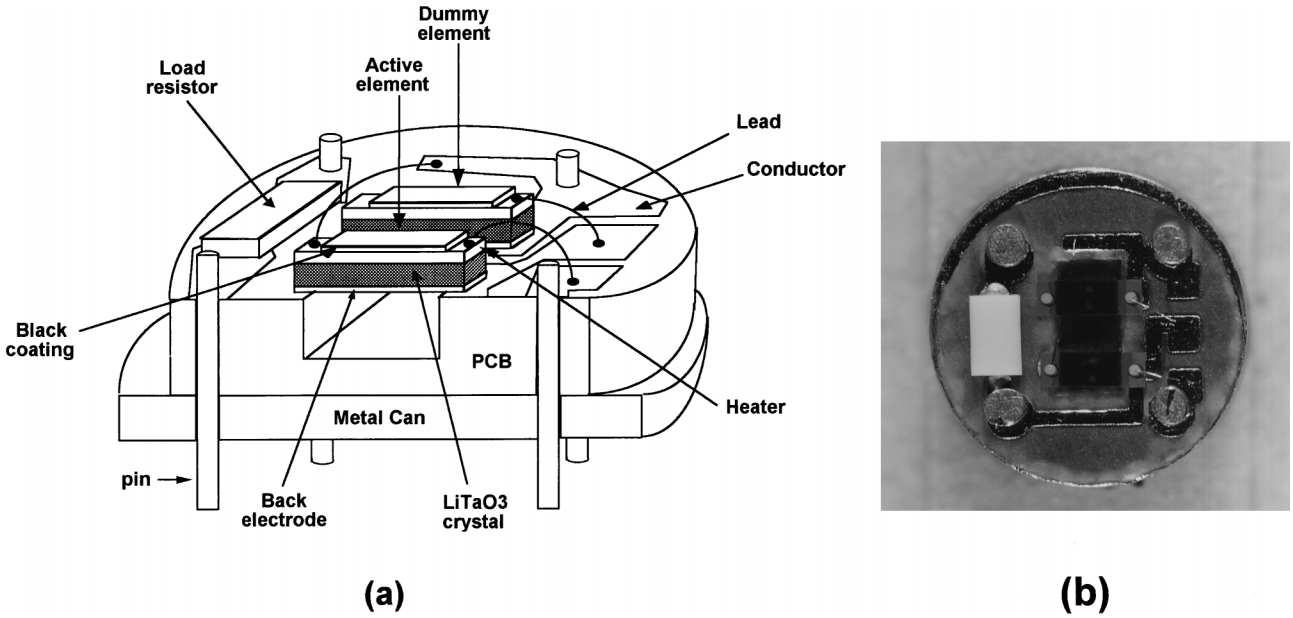

Fig. 4. Configuration of the fabricated electrically calibrated pyroelectric detector: (a) cross section, (b) bird's-eye view.

tector structure is very similar to that used in the current commercial pyroelectric tympanic thermometer,[5] except the active element is coated with a thin-film heater (~600 Ω) on its upper surface. The dummy element is shielded from illumination by an opaque mask over it. To reduce the microphonic effect, the polarizations of the active and dummy sensors are arranged in opposite directions to cancel the piezoelectrically induced charges.

B. Circuits

The circuit for electrical calibration is depicted in Fig. 5(a). An energy-storage capacitor of 2000 uF, C_{ref}, is used for reference heating. The capacitor is precharged by Vcc through switch S1 (CD4053) at the P1–P1′ positions. After switching to the P2–P2′ positions, the capacitor starts to heat the active element through the heating resistor Rh. As shown in Fig. 5, isolation of the capacitor during heating ensures that the detector output signal is free from any false signal that might be fed through the detector capacitance if the detector were directly heated by Vcc. The capacitor-isolated-heating configuration therefore improves the power supply rejection ratio (PSRR) of the measurement significantly. A 1-Ω resistor Rs in series with the heater Rh is used to read the heating current for the electrical power calculation. A variable resistance Rb between P2 and P2′ is used to ensure that the sensor output voltage is referred to the preamplifier (A1) ground through a balanced bridge configuration, because the ground potential of the active sensor on heater electrode Rh is floating and is not accessible.[19–21]

The induced weak pyroelectric current is converted to a voltage through preamplifier A1. A large load resistor R_q mounted inside the package is used as the feedback resistor to the preamplifier to increase the gain. An AD590M IC is used to sense accurately the ambient temperature by the proportional-to-absolute-temperature method.[22] This is of paramount importance for the accuracy of the thermometer as indicated in Eq. (22). Figure 5(b) shows the timing sequence of the operation.

C. PSPICE Simulation

Using the opto-electro-thermal model established above, we are able to simulate the behavior of any pyroelectric tympanic thermometer. Two cases are studied, the conventional non-ECP method and the present ECP method. The device parameters were extracted by the bolometric method previously used in our laboratory,[18,19] which gives the following data: $p = 6 \times 10^{-9}$ C/cm^2, $\mathcal{G} = 0.0008$ W/°C, $\mathcal{H} = 0.003$ J/°C, and $\Re_v = 1252$ V/W. We calibrate the $\Re_v$ value of the tested sample by referring to a blackbody at 37 °C.

Figure 6 shows the results of the simulation. We vary the pyroelectric constant and thermal conductance by 50% to allow for practical deviations in manufacturing. For a thermometer using a conventional non-ECP sensor, the measured temperature could deviate over several tens of degrees away from the assumed true temperature of 37 °C. This is much larger than the medical allowance of 0.1 °C described above. Curve (a) in Fig. 6 indicates that if the pyroelectric constant were changed by only 1%, the measured temperature would be in error by 0.216 °C. Similarly, the error is 0.181 °C for a change of 1% in the conductance as seen in curve (b). The simulation thus proves that the measured temperature is very sensitive to variations in the device parameter, which cannot be avoided in real situations. Therefore precise in-factory calibration and a good circuit design are necessary to compensate for the parameter variations of the individual detectors and the aging of the detector material in chronic use of a tympanic thermometer.

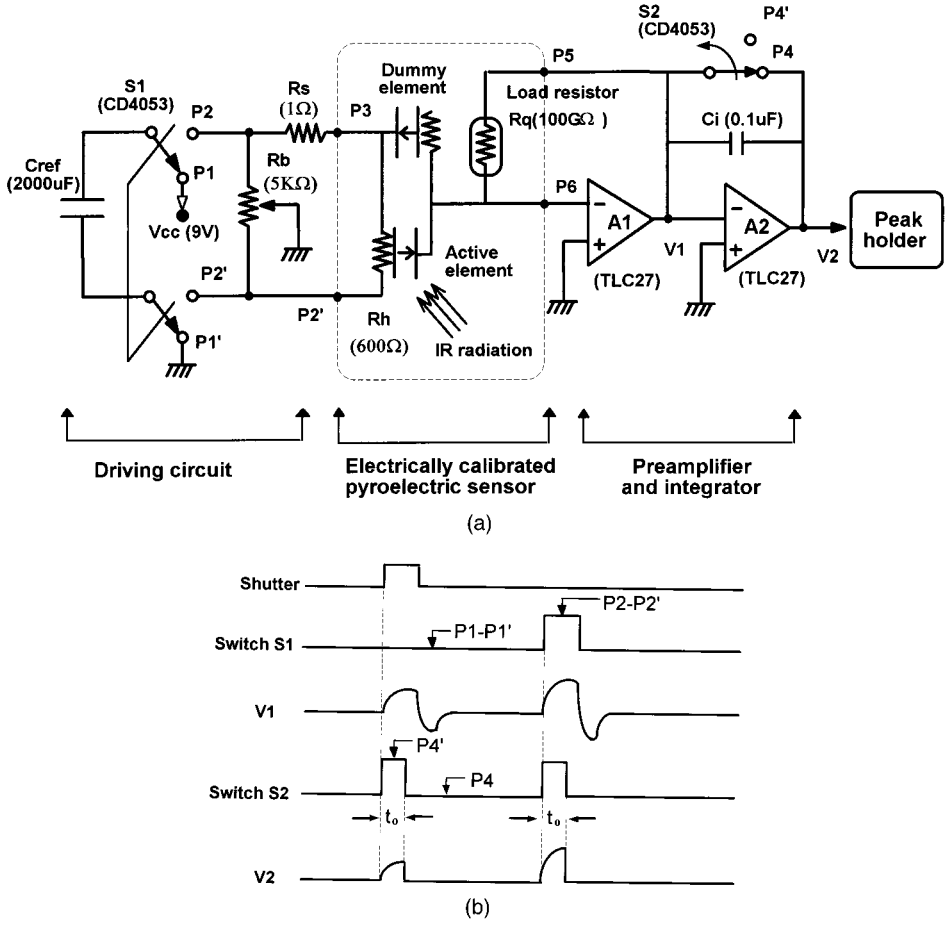

Fig. 5. (a) Readout and calibration circuits including driving circuit, ECP, and dummy sensors, preamplifier, integrator, and peak holder. (b) Timing diagram.

Curve (c) of Fig. 6 also shows the results of the simulation of the present ECP thermometer, where differences in the device parameters of the two pyroelectric elements are allowed. It is evident that the ECP method is independent of device variation as predicted by the theory.

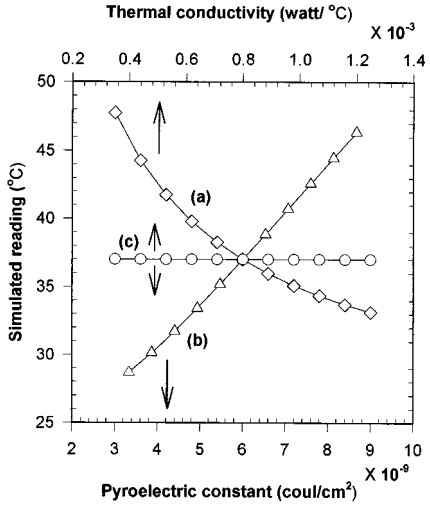

Fig. 6. Simulation results of the model in Fig. 2 showing the relation of the measured temperature to the thermal conductance and pyroelectric constant. A measured temperature of 37 °C is set to represent a human's eardrum when the device parameters are $p = 6 \times 10^{-9}$ C/cm^2, $\mathcal{G} = 0.0008$ W/°C, $\mathcal{H} = 0.003$ J/°C, and $\Re_v = 1252$ V/W.

D. Experimental Measurements

Using the fabricated ECP sensors in Fig. 4 and the circuits shown in Fig. 5, we are able to test the

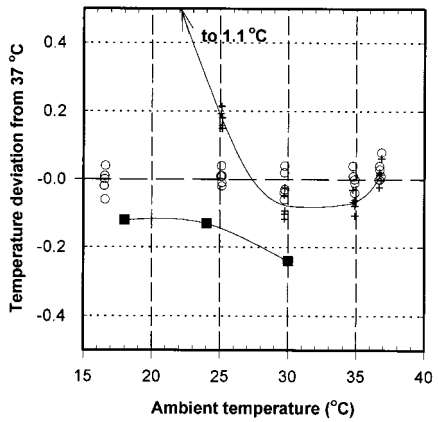

Fig. 7. Measurement errors as a function of ambient temperature. Cross points are from our thermometer without the ECP method being utilized. Circles are from the present ECP method, and solid squares are the data taken by Cascetta[8] from a commercial tympanic thermometer.

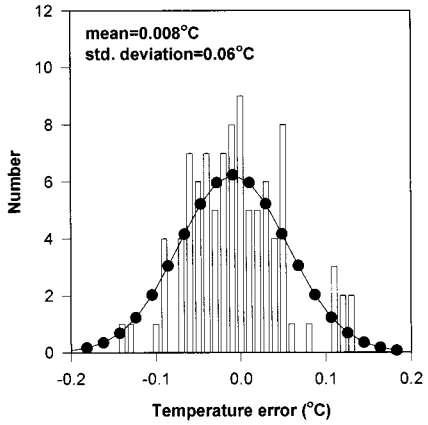

Fig. 8. Error distribution of 100 experiments in various conditions. The mean error is 0.008 °C, and the standard deviation is 0.06 °C. These results imply that each measurement has a 90% confidence for an accuracy within 0.1 °C.

ambient-temperature effect of our ECP tympanic thermometer. The tympanic thermometer is set up in front of a reference blackbody, which simulates the human eardrum at 37 °C. The measured values were recorded while the ambient temperature changed from 17 to 37 °C. The results are shown in Fig. 7. The vertical axis represents the measured temperature relative to 37 °C. The square points represent the data from the commercial tympanic thermometer described by Cascetta.[8] The cross points are from the device described here without use of the ECP method, while the circles are for the same device with the ECP method. Note that the electrically calibrated tympanic thermometry is superior to the other two methods and is able to meet the clinical criterion of 0.1 °C accuracy across a wider ambient temperature range. Also shown in Fig. 8 is the error distribution for 100 measurements in various situations, including different ambient and core temperatures. A normal distribution is used to fit these data, which gives a calculated mean and a standard deviation of 0.008 and 0.06 °C, respectively. This means that the present ECP thermometer has an accuracy of 0.1 °C with 90% confidence. These results show that the ECP method is effective and reliable when applied to tympanic thermometry.

5. Conclusion

A new tympanic thermometer utilizing a modified ECPR technique has been analyzed theoretically and demonstrated experimentally. This method is not influenced by ambient temperature and detector aging and is able to provide the accuracy required by clinical applications. The theoretical analysis provides a base for establishing an integrated opto-electro-thermal PSPICE model capable of simulating the tympanic thermometer. This model can be modified to accommodate other thermal detectors[18] and applied to other applications relating to radiation thermometry.

The authors are obliged to Opto Tech Corporation and Oriental System Technology Inc. in Hsinchu Science-Based Industrial Park for invaluable technical support in the fabrication of the pyroelectric sensor package and the experimental setup, respectively.

References

1. J. G. Webster, *Encyclopedia of Medical Devices and Instrumentation*, *Vol. 4* (Wiley, New York, 1988), pp. 2723–2730.
2. T. H. Benzinger, "On physical regulation and the sense of temperature in man," Proc. Natl. Acad. Sci. **45,** 645–649 (1959).
3. M. Benzinger, "Tympanic thermometry in anesthesia and surgery," J. Am. Med. Assoc. **209,** 1207–1211 (1969).
4. G. J. O'Hara and D. B. Phillips, "Method and apparatus for measuring internal body temperature utilizing infrared emissions," U.S. patent 4,602,642 (29 July 1986).
5. J. Fraden, "Infrared electronic thermometer and method for measuring temperature," U.S. patent 4,797,840 (10 January 1989).
6. J. Jakobsson, A. Nilsson, and L. Carlsson, "Core temperature measured in the auricular canal: comparison between four different tympanic thermometers," Acta Anaesthesiol. Scand. **36,** 819–824 (1992).
7. M. E. Weiss, A. F. Pue, and J. Smith III, "Laboratory and hospital testing of new infrared tympanic thermometer," J. Clin. Eng. **16,** 137–144 (1991).
8. F. Cascetta, "An evaluation of the performance of an infrared tympanic thermometer," Measurement **16,** 239–246 (1995).
9. J. Geist and W. R. Blevin, "Chopper-stabilized null radiometer based upon and electrically calibrated pyroelectric detector," Appl. Opt. **12,** 2532–2535 (1973).
10. W. M. Doyle, B. C. Mcintosh, and J. Geist, "Implementation of a system optical calibration based on pyroelectric radiometry," Opt. Eng. **15,** 541–548 (1976).
11. F. Hengstberger, *Absolute Radiometry: Electrically Calibrated Thermal Detectors of Optical Radiation* (Academic, New York, 1989), pp. 1–116.
12. J. Fraden, "Noncontact temperature measurements in medicine," in *Bioinstrumentation and Biosensors* (Marcel Dekker, New York, 1991), pp. 511–549.
13. A. K. Oppenhein, "Radiative analysis by network method," Trans. Am. Soc. Mech. Eng. **78,** 725–735 (1956).
14. J. P. Holman, *Heat Transfer*, 7th ed. (McGraw-Hill, New York, 1992), pp. 385–506.
15. R. D. Hudson, *Infrared System Engineering* (Wiley, New York, 1969), pp. 20–113.
16. J. Copper, "Minimum detectable power of a pyroelectric thermal receiver," Rev. Sci. Instrum. **33,** 92–95 (1962).
17. M. Simbony and A. Shaulov, "Pyroelectric voltage response to step signals of infrared radiation in triglycine sulphate and strontium-barium niobate," J. Appl. Phys. **42,** 3741–3744 (1971).
18. J. S. Shie, Y. M. Chen, M. Ou-Yang, and B. C. S. Chou, "Characterization and modeling of metal-film microbolometer," IEEE J. Microelectromech. Syst. **5,** 298–306 (1996).
19. M. Ou-Yang, "Implementation of absolute optical power meter with single-chip controller," M.S. thesis (National Chiao Tung University, Taiwan, 1993).
20. J. S. Shie, J. C. Hong, and G. H. Yu, "Design of electrically calibrated pyroelectric radiometer," J. Chin. Inst. Eng. **12,** 239–247 (1989).
21. R. J. Phelan and A. R. Cook, "Electrically calibrated pyroelectric optical–radiation detector," Appl. Opt. **12,** 2494–2500 (1973).
22. M. P. Timko, "A two-terminal IC temperature transducer," IEEE J. Solid-State Circuits **SC-11,** 784–788 (1976).